JOURNAL OF SOLID STATE CHEMISTRY 93, 316–330 (1991)

High Resolution Electron Microscopy Study of Defects in "High Oxygen Pressure" $YBa_2Cu_4O_8$

B. DOMENGÈS, M. HERVIEU, AND B. RAVEAU

Laboratoire CRISMAT, Boulevard du Maréchal Juin, 14050 Caen Cedex, France

AND J. KARPINSKI, E. KALDIS, AND S. RUSIECKI

Laboratorium für Festkörperphysik, ETH Hönggerberg/HPF, CH-8093 Zürick, Switzerland

Received December 10, 1990; in revised form March 11, 1991

This paper deals with the high resolution electron microscopy study of $YBa_2Cu_4O_8$ samples prepared under high oxygen pressure. Many different types of defects, which differ either by their nature or frequency from those observed in samples prepared by different technics, such as stacking defects involving 90° rotated domains or change in periodicity, have been encountered. The existence of a new stacking sequence, $YBa_3Cu_4O_9$, is suggested. © 1991 Academic Press, Inc.

Introduction

Since the first observations by high resolution electron microscopy (HREM) of layers of $(CuO)_2$ double rows in superconducting $YBa_2Cu_3O_7$ (*1*, *2*), the ordered stacking $Y–CuO_2–BaO–(CuO)_2–BaO–CuO_2–Y$ has been stabilized in thin films (*3*, *4*) then in bulk ceramics $YBa_2Cu_4O_8$, which first could be synthesized under high oxygen pressures (*5*, *6*). Other techniques have been studied based on either the melted mixture procedure (*7*) or the direct synthetic route (*8*) which allow a critical temperature of 80 K to be reached. Furthermore, $YBa_2Cu_4O_8$ appears a good candidate to high J_c current since oxygen stoichiometry is easier to control than in $YBa_2Cu_3O_7$. A microstructural study related to the synthesis process is of interest because defect microstructure seems to influence the pinning characteristics of the YBaCuO materials (*9*, *10*). HREM studies of $YBa_2Cu_4O_8$ and $YBa_2Cu_3O_7$ thin films have tried to correlate electrical performances and microstructure, i.e., ion orderings, defect density following the idea that some defects such as stacking faults may play a role in flux pinning (*11–14*). To compare with bulk ceramics prepared by other routes (*15–18*), the following study characterizes the microstructure of $YBa_2Cu_4O_8$ ceramics prepared by the high oxygen pressure method (*5*).

Experimental

The synthesis of this sample was performed in two steps. A pellet of a homogeneous mixture of **123** and CuO was subjected to oxygen pressure of 500 bar and

0022-4596/91 $3.00
Copyright © 1991 by Academic Press, Inc.
All rights of reproduction in any form reserved.

1000°C reacting to form **124.** The oxygen pressure was then released and the material was cooled to room temperature. In this way, a partial decomposition of **124** took place. Next, the oxygen pressure was increased again up to 500 bar and the material annealed at 1000°C. Cooling took place under pressure. The sample homogeneity was tested by X-ray powder diffraction and Guinier camera film showed an almost pure **124** phase. For electron microscopy study, samples were slightly grounded in *n*-butanol to avoid induced fractures and deposited on a holey carbon coated grid. Electron diffraction (ED) was performed on a JEM 120CX equipped with a side-entry goniometer and high resolution work (HREM) on a JEM 200CX equipped with a top-entry stage using a double tilt goniometer (±10°) and an objective lens with a spherical aberration constant C_s = 0.8 mm, which leads to a theoretical resolution of 0.22 nm. The multislice method was used to calculate high resolution images (*19*). Magnetic measurements have shown a sharp transition (<5 K) with a T_c of 80 K and a large diamagnetic volume fraction over 60%.

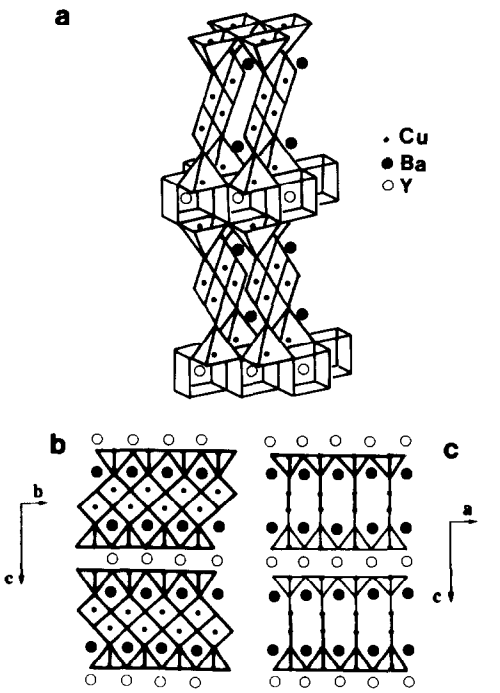

FIG. 1. (a) Perspective view; (b) [100] and (c) [010] projections of $YBa_2Cu_4O_8$ structure. In the latter, (CuO_2) slabs differing by a translation of **b**/2 appear with lighter lines.

Structural Recalls

$YBa_2Cu_4O_8$ structure (*6, 20*) can be described through the introduction of an additional $[CuO]_\infty$ row between the $[BaO]_\infty$ layers of the $YBa_2Cu_3O_7$ structure (*21*); the single $[CuO]_\infty$ rows of corner-sharing CuO_4 square groups are then replaced by double $[(CuO)_2]_\infty$ rows of edge-sharing CuO_4 groups (Fig. 1), similar to those observed in $SrCuO_2$ (*22*). This structural unit appears to be highly stable and it is worth noting that up to now attempts to substitute A^{III} or A^{I} for Sr^{II} in $SrCuO_2$, which would allow a variation of oxygen stoichiometry, have failed.

Electron Diffraction Results

About 50 crystals were characterized by electron diffraction. All of them, except three identified as **123**-type crystals and two as $Y_2Cu_2O_5$ fragments (*23*), showed the parameters ($a \approx b \approx a_p$, $c \approx 2.75$ nm) and the reflection conditions (hkl: $k + l = 2n$) of the **124**-type structure. Besides the few crystals appearing defect free, most of them showed diffraction patterns and thus low resolution images typical of several types of disorders: diffusion streaks parallel to the *C* axis related to stacking defects; superimposition of ED patterns or simple splitting of dots, i.e., presence of domains; diffusion streaks forming arcs perpendicular to the *C* axis, i.e., rotated zones about *A* or *B* axis; amorphous areas (Fig. 2). These phenomena appear more or less intense on the ED patterns and thus more or less extended on the corresponding images. The point is that most crystals show disorders or one will observe

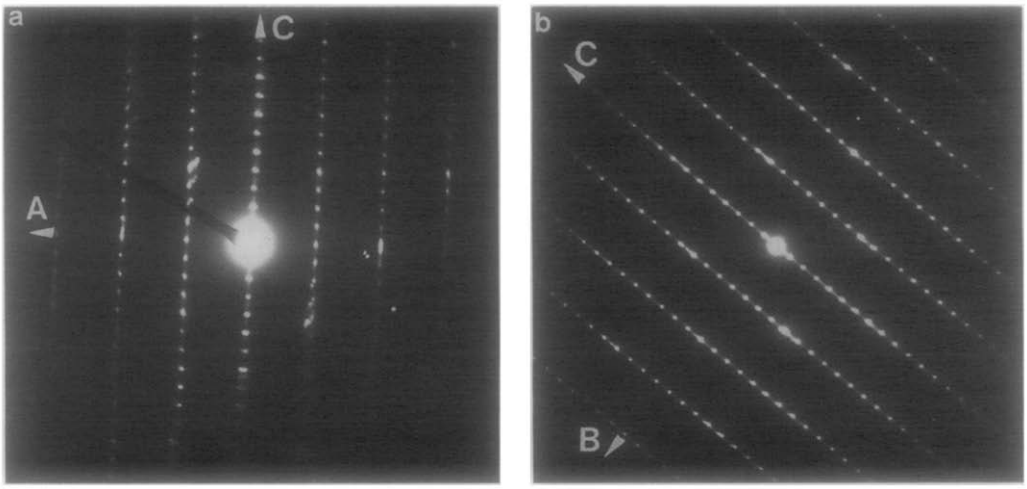

FIG. 2. Typical electron diffraction patterns of $YBa_2Cu_4O_8$ crystals. (a) [010] ED pattern shows diffusion streaks forming arcs characteristic of domains rotated about B axis. (b) [100] ED pattern shows diffusion streaks parallel to C axis characteristic of stacking defects.

in the same crystal a very regular zone which may be wide but beside defective ones. Some of these features are described in the next section.

High Resolution Electron Microscopy Results

Owing to the anisotropic character of the **124** structure (Fig. 1), the [100] and [010] directions of observation have been mostly chosen to characterize this sample, especially stacking defects. In order to interpret observed contrasts, image calculations have been performed. Figure 3 gives through-focus series calculated for both directions. Characteristic images allow the two orientations to be easily distinguished, depending on the direction of the electron beam toward the $(CuO)_2$ slabs: long bright dots or the zig-zag disposition of bright dots when the electron beam is parallel or perpendicular to the $(CuO)_2$ slices, respectively. Experimental images are in good agreement with calculated ones (Fig. 4). For a defocus value close to Scherzer (≈ -40 nm), bright dots are related to the low electron density zone of the structure, i.e., oxygen atoms and tunnels: brighter dots are those associated with oxygen vacancy in the yttrium plane and the zig-zag ones to oxygen atoms of the $(CuO)_2$ slabs on (100) images, whereas on (010) ones, tunnels between square planar $(CuO)_2$ rows appear as long bright dots. Twenty-three crystals have been observed by high resolution electron microscopy. Very few of them appear regular in agreement with electron diffraction investigation.

Extended Disorders

Most crystals are characterized by extended disorders. In Fig. 5a, a wide area of the crystal is regular but an amorphous area can be seen on the edge and strain contrast is associated with disoriented domains. When referred to the exact observation orientation, misorientation may result in a rotation around an axis either parallel or perpendicular to the observation directions ([010]

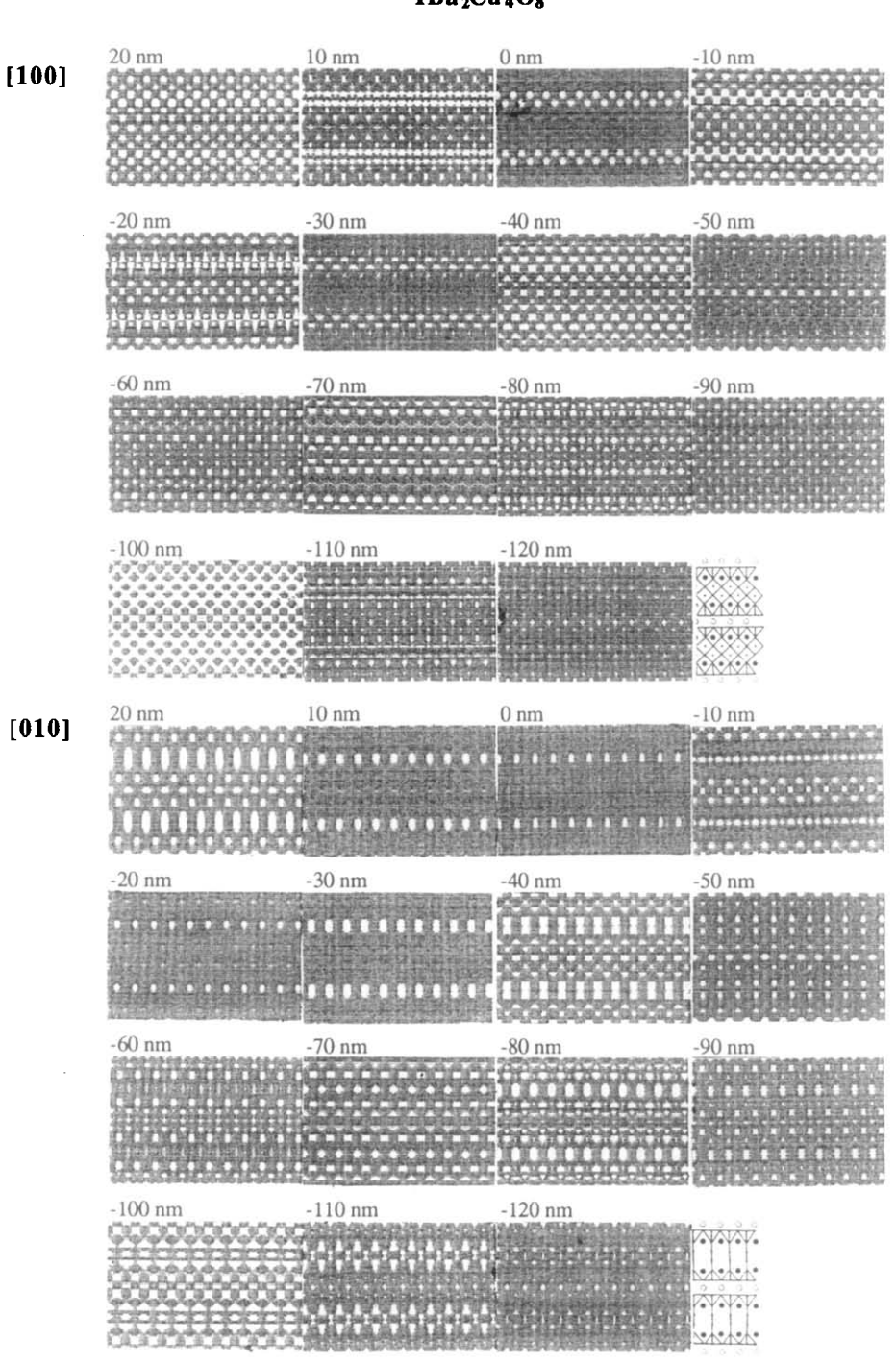

FIG. 3. Calculated [100] and [010] through-focus series. Parameters are: high voltage, $V = 200$ kV, crystal thickness $T \approx 3$ nm, spherical aberration constant $C_s = 0.8$ mm, 131 beams in the objective aperture, convergence half-angle $\alpha/2 = 0.8$ mrad, depth of focus $\Delta/2 = 7.5$ nm.

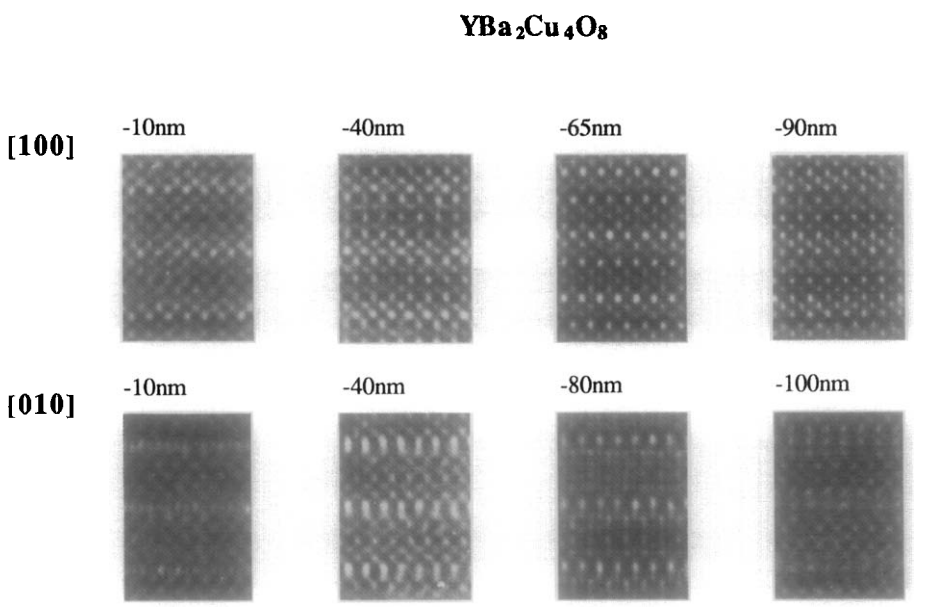

FIG. 4. Typical images of experimental [100] and [010] through-focus series.

and [100]), i.e., to the microscope axis. When parallel to it, the angle of rotation generally varies from 1 to 14°, and rarely to 30°. When perpendicular to the microscope axis, disorientation makes it very difficult and rather rare to orientate perfectly an entire crystal and the contrast varies rapidly from one area to another, though following the edge of the crystal (Fig. 5b). More evidence of inner disorders is the frequency of monoclinic distortions, which may be as large as 1°. The crystal of Fig. 6 shows a 0.6° monoclinic distortion on its ED pattern and resolution image. Corresponding to the splitting of spots on the ED pattern, several disoriented domains appear along the edge of the crystal and Moiré patterns are observed at the junction and superimposition of these domains.

Stacking Disorders

Besides these disorders, which can be considered as growth defects, some appear localized and involve the ordering of slab stacking in the $YBa_2Cu_4O_8$ structure. Two types of stacking faults (SF) can be considered: the first is described by the change in direction of slab stacking; the second corresponds to the change in the stacking sequence.

(*i*) *Change in direction.* As an example of the first type of SF, the crystal image in Fig. 7 shows an **a** × **c** slab in a **b** × **c** matrix. This defective slab extends throughout the crystal. As schematized in Fig. 8, this change in direction appears even easier than in the **123** structure (*24*), because of a **b**/**a** ratio closer to 1 in the **124** structure and (001)-oriented domains were expected. But contrary to samples prepared under low oxygen pressure where (001)-oriented domains were often observed (*18*), this defect, i.e., change in direction, remains isolated in an almost regular crystal. Indeed, ED patterns built up from the superimposition of **A** × **C** and **B** × **C** patterns observed by Krekels *et al.* (*18*) have never been encountered. This

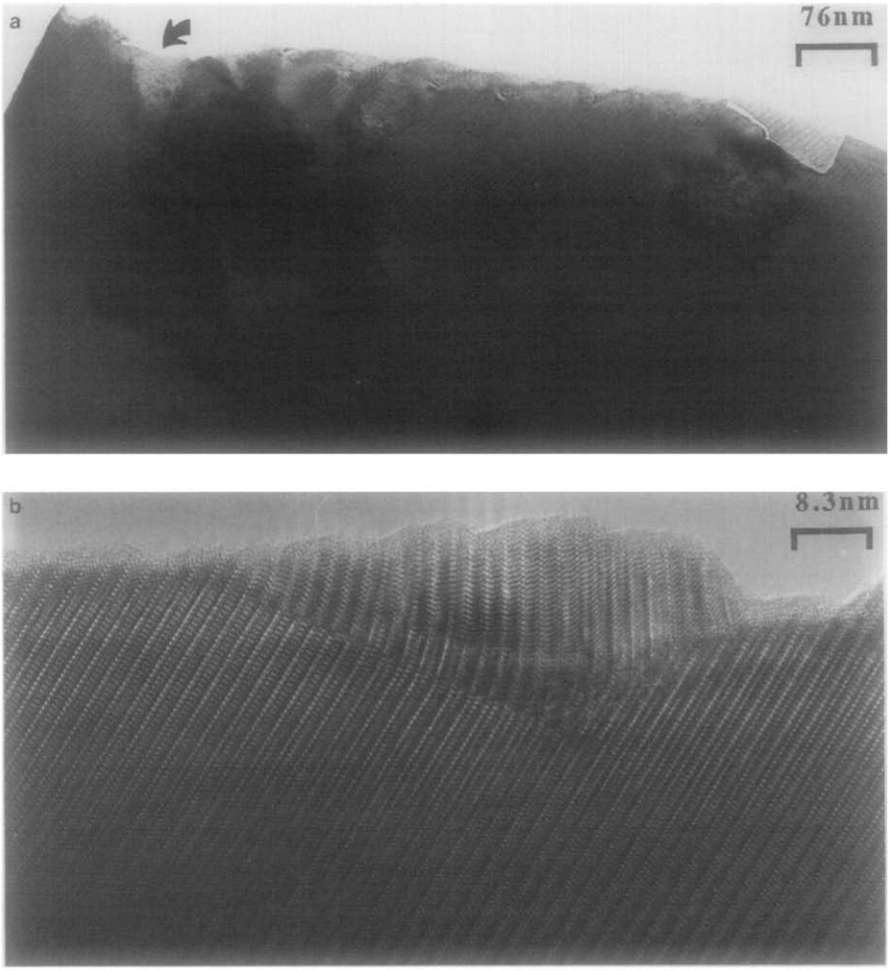

FIG. 5. (a) [010] low magnification image showing two disordered domains in a regular crystal. Ill-crystalized area is observed on the edge (arrow). (b) [010] high resolution image showing both types of rotated domains. From left to right part of the crystal edge, contrast varies rapidly and an outgrowth is rotated 30° about the *B* axis.

feature confirms, if needed, the influence of the synthesis method on microstructure.

Reversal in direction has been observed on (010) images (Fig. 9). It is located close to the edge of the crystal. Following the double copper rows, the image contrast clearly shows that CuO_4 square groups are 90° oriented from the left to the right, with a relaxed intermediate zone leading to distortion of the neighboring framework. This strong disturbance can be easily understood, taking into account the framework modifications implied by such a rotation. A model for the $(100)_P$ boundary can be proposed (Fig. 10a). To study precisely the nature of this boundary, it appears useful to project each layer parallel to [001]: the first pyramidal layer remains unchanged (Fig. 10b). At a square group level, a complex cluster of copper polyhedra is built up from

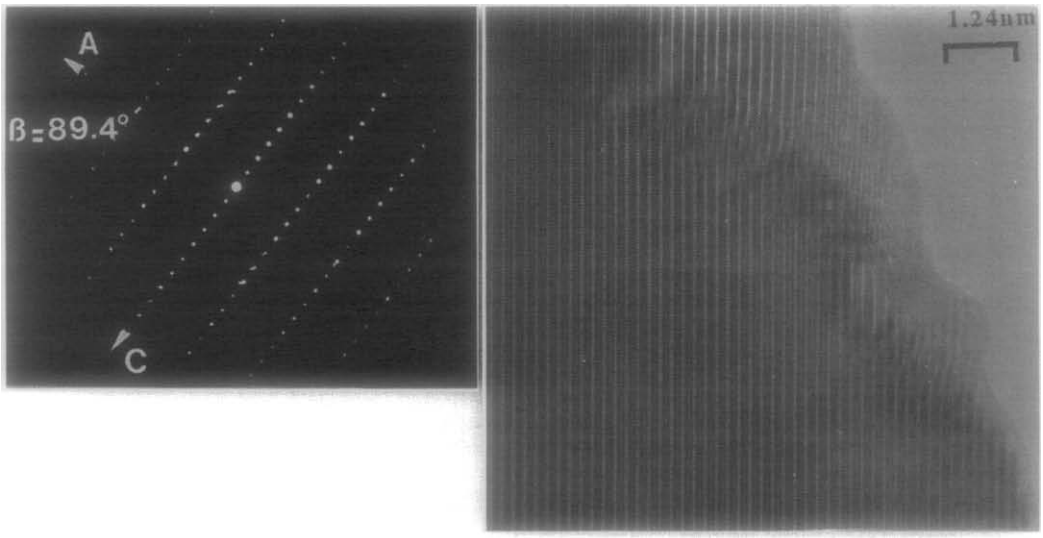

FIG. 6. [010] ED pattern and image. Monoclinic distortion is observed and the splitting of ED dots is related to rotated domains which result in Moiré patterns at their junction.

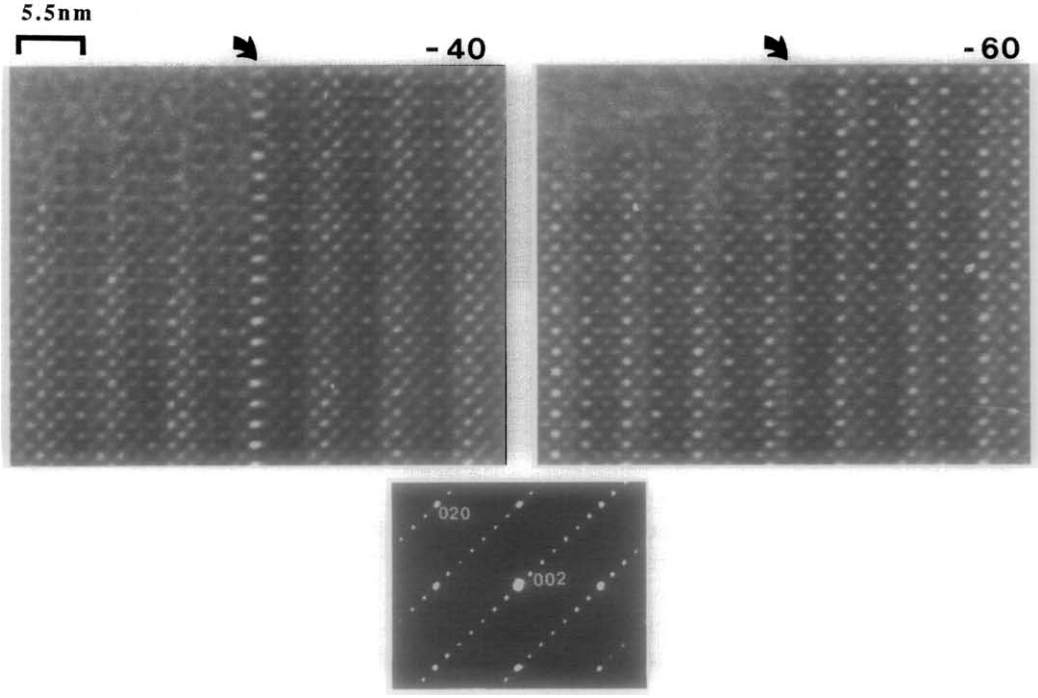

FIG. 7. [100] high resolution images (D_f close to -40 and -60 nm) and ED pattern. An **a** × **c** slab (arrow) is observed in the **b** × **c** matrix without perturbation of the neighboring framework.

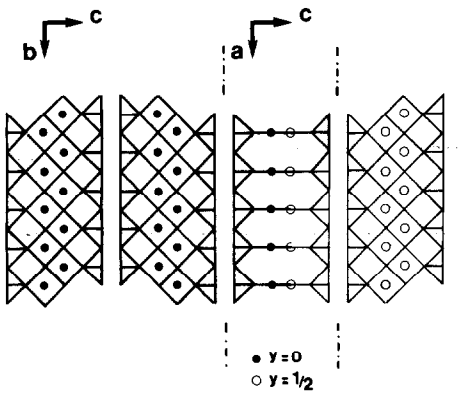

FIG. 8. Idealized projection of previous stacking defects, i.e., [001] oriented domains. In Figs. 8 to 11, center copper atoms are drawn differently: black dots and empty circles symbolize copper atoms in and out of the sheet plane, respectively.

one pyramid sharing edges with three CuO_4 groups, two on the basal plane of the pyramid (Fig. 10c), thus implying the formation of a double row of edge-sharing pyramids in the second pyramidal layer (Fig. 10d); there is the remaining problem of the junction of this disturbed pyramidal layer with adjacent ones in the neighboring slabs, all being spaced through an $[Y]_\infty$ layer. Observations show that this change in direction appears at the very edge of the crystals where relaxation of the framework is easier and the number of layers of the structure involved in the junction is lower. In the same way, the size of the relaxed intermediate zone related to the low thickness of the crystal led us to propose another junction model based on a boundary parallel to $(110)_P$ (Fig. 11). As noted above, [001] projection allows the precise study of the junction layer to layer: the first pyramidal layer remains unchanged; at a square group level, one of the $[CuO]_\infty$ rows changes in direction through the formation of one single copper polyhedron row (octahedra Fig. 11a, pyramids Fig. 11b), in a similar way to (110) twin boundaries in $YBa_2Cu_3O_7$, and in the second one, two 90°-oriented square groups are corner-shared; in the second pyramidal layer, blocks of edge-sharing pyramids are built up parallel to the $(110)_P$ boundary. These complex models probably give a good description of the clusters involved in the junction between 90°-rotated domains (Fig. 12) but they also reflect, in agreement with the observations, the disturbance it introduces on the neighboring **124** framework, which confines this SF defect to the very thin edges of the crystals.

(ii) Change in the periodicity. No **123** stacking fault was observed, contrary to the study of Yamaguchi *et al.* (*15*). In fact, the two samples differ by the oxygen pressure during synthesis, 200 bar in Yamaguchi's against 400 bar in ours.

Among the 23 studied crystals, 5 pieces showed a type of defect which involves an extra $[AO_y]_\infty$ layer, with the nature of the *A* cation to be elucidated. In the [100] crystal image of Fig. 13, the **c** periodicity is not the same all over the matrix. Indeed, three wider layers are observed. Beginning from the edge of the crystal, the periodicity is –1.36 nm–1.52 nm–1.52 nm–1.36 nm–1.52 nm–1.36 nm–1.36 nm–. . . . One of the problems in the identification of these defective slabs is that, despite very similar contrast, the width of the slab may vary from 1.47 to 1.52 nm ($\sigma = \pm 0.02$ nm) and not from one crystal to the other, but from one area to the other in the same fragment. In two crystals, this type of slab becomes so frequent that ED pattern indicates a $0.38 \times 1.5\text{-nm}^2$ periodicity instead of 0.385×2.74 nm^2, with diffusion streaks due to the coexistence of both arrays (Fig. 14). The careful analysis of contrast, especially with the presence of three rows of brighter dots instead of two in zig-zag associated with the $(CuO)_2$ planes in $YBa_2Cu_4O_8$ structure, suggests the insertion of an extra $[AO_y]_\infty$ layer.

Two fundamentally different models may be retained. The first was proposed earlier when a similar isolated defect was observed

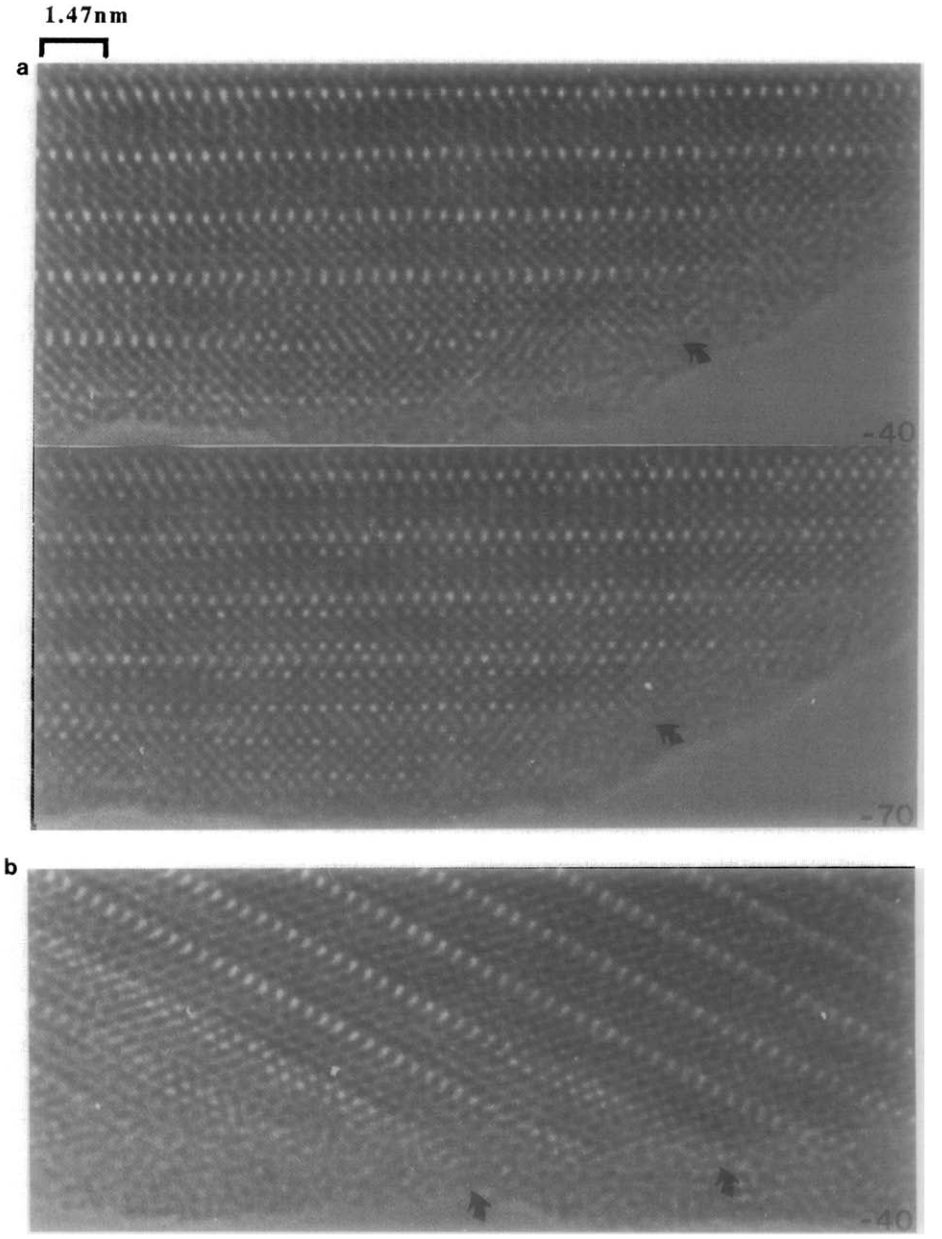

FIG. 9. [010] high resolution images of two crystal edges showing a change in the direction of the $(CuO)_2$ square planar groups. (a) Two focused images are provided, -40 and -70 nm. (b) The phenomenon is observed in two slices (arrows). Note that these SF occur at the very edge of the crystals after a localized perturbation of the framework.

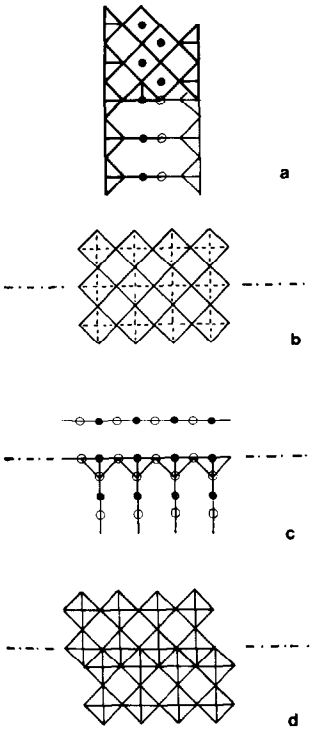

FIG. 10. Schematized model of $(100)_P$ boundary. (a) Projection along **b** or **a** (b, c, and d) [001] projection layer by layer.

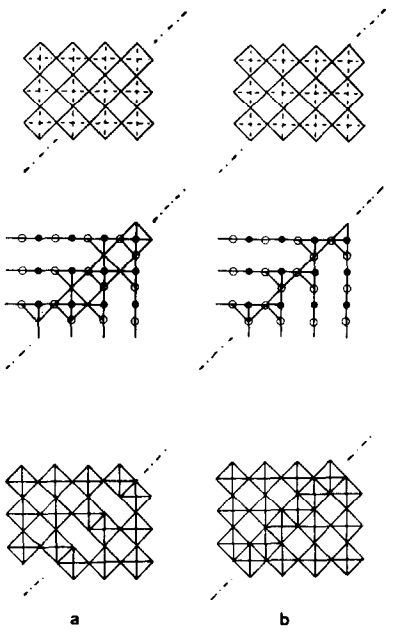

FIG. 11. Schematized model of $(110)_P$ boundary projected layer by layer parallel to [001]. At square group level, the junction involves either octahedra and pyramids (a) or pyramids only (b).

in a $YBa_2Cu_3O_{7\pm\varepsilon}$ matrix by high resolution electron microscopy on ceramic samples (*25*, *26*) and recently on laser-deposited Y–Ba–Cu–O thin films (*11*, *12*). Every author agrees on most atom stacking [Y – CuO_2 – BaO – CuO_y – AO – CuO_y – BaO – $(CuO)_2$–Y] (Fig. 15). Ramesh *et al.* (*11*, *12*), following Ourmazd *et al.* (*25*), propose y = 1 and A = Y leading to the composition $Y_2Ba_2Cu_4O_9$ (Fig. 15a). This model seems to us unfavorable. Indeed, in this model the yttrium site between CuO chains would be characterized, despite an eightfold oxygen coordination, by Y–O bond lengths much longer (0.27 nm) than those of the usual Y site (0.24 nm). The YO_8 as-built cage would be thus strongly elongated (0.38 × 0.29 nm^2). Such a distorted cage appears unlikely

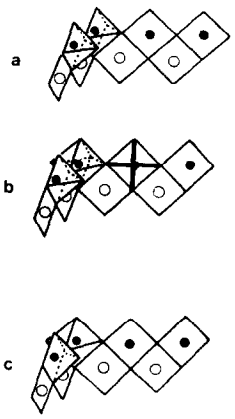

FIG. 12. Perspective views of clusters formed in the $(CuO)_2$ layers of previous models. (a) $(100)_P$ boundary through pyramids sharing the same base plane, (b and c) $(110)_P$ boundary through one octahedron and two perpendicular pyramids or one octahedron and one pyramid, respectively.

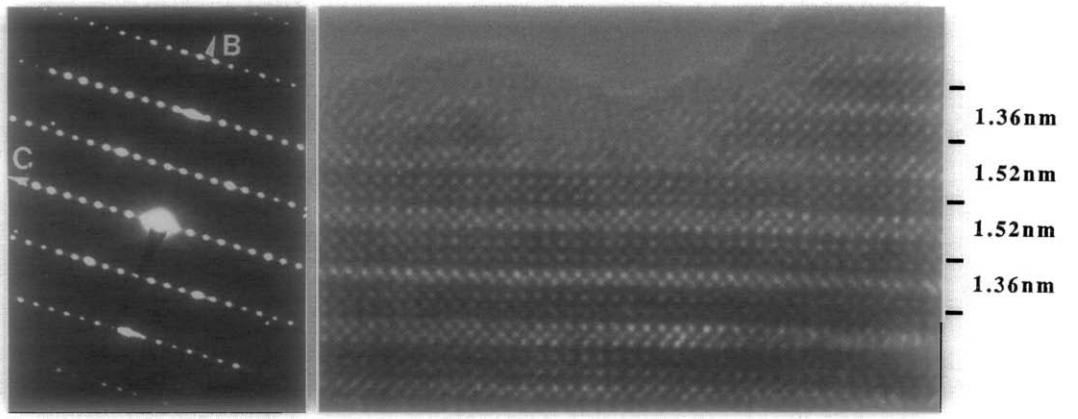

FIG. 13. [100] high resolution image showing slabs of 1.52 nm width instead of $c/2 = 1.36$ nm. Dots are elongated parallel to **C** on the corresponding ED pattern.

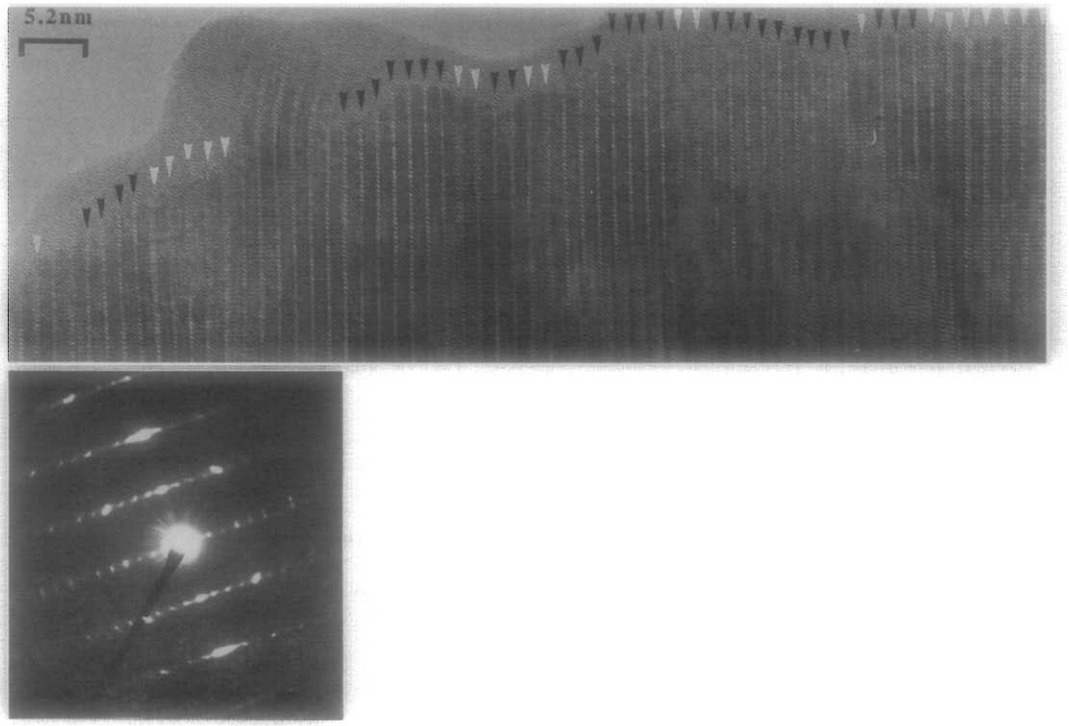

FIG. 14. [010] high resolution image and ED pattern of a disordered crystal. ED pattern dots can be indexed in a $0.38 \times 1.5\text{-nm}^2$ cell. Corresponding to diffusion streaks, the intergrowth of 1.36 nm (black arrows) and 1.52 nm wide (white arrows) slabs is observed on the crystal image.

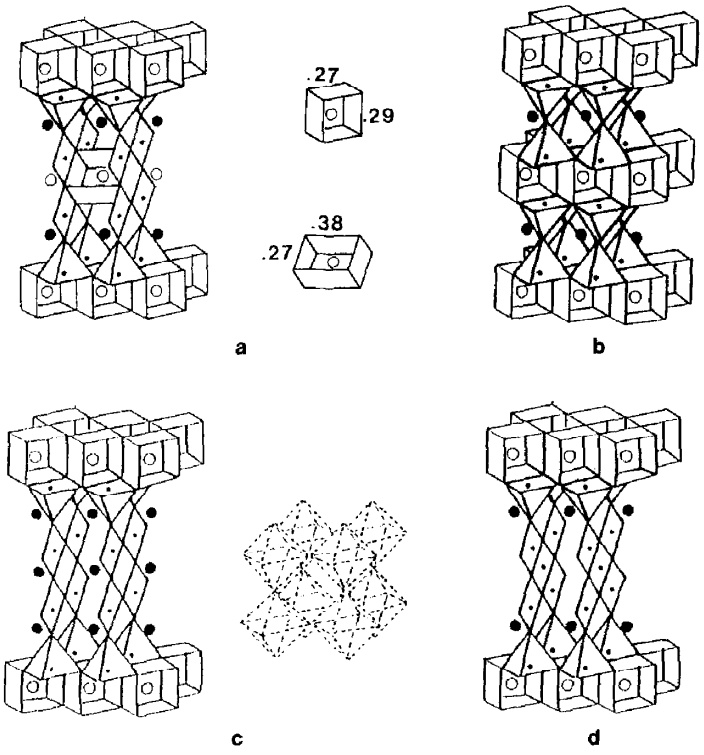

FIG. 15. Perspective views of different models for previous stacking fault: (a) $Y_2Ba_2Cu_4O_8$, the size of both yttrium cages is given in nanometers; (b) $YBaCu_2O_5$; (c) $YBa_3Cu_4O_{9\pm\varepsilon}$, statistical oxygen occupancy around center copper atoms appears more likely; (d) $YBa_2Cu_5O_9$.

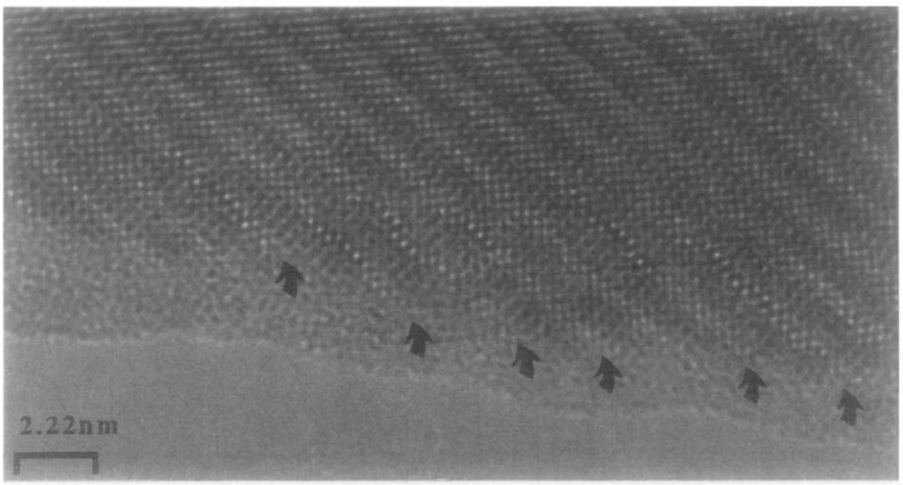

FIG. 16. [100] high resolution image taken at focus close to −40 nm showing original contrast at the level of $(CuO)_2$ square planar groups (arrowed).

for Y which is generally located in the symmetrical AO_8 cage (the distance between $(CuO)_2$ square planes in the fluorine-type cage is lowered to 0.29 nm in $YBa_2Cu_3O_7$ and $YBa_2Cu_4O_8$ structures). Moreover the tendency of Y to adopt a pseudocubic environment would involve short O–O distances and then too short Cu–Cu distances. In layered cuprates built up from the intergrowth of rock-salt layers and double pyramidal layers ($m = 2$), this tendency of Y is compensated by a displacement of the Cu atoms toward the apical oxygen of CuO_5 pyramids; this is impossible when additional $[ACuO_2]_\infty$ slabs are inserted between the pyramidal layers ($m \geq 3$) and indeed, Y-doped cuprates with $m \geq 3$ have not yet been observed. To ensure a proper environment for Y, another model would consist of Cu_2O_9 bipyramids, leading to the composition $YBaCu_2O_5$ (Fig. 15b), which would thus be isostructural to $YBaFeCuO_5$ (*27*). The latter could only be stabilized with 50% Fe in the copper sites. Thus, stabilization of Cu_2O_9 bipyramids in $YBaCu_2O_5$ seems also unfavorable. We prefer the model proposed earlier with A = Ba and y close to 1 (Fig. 15c): $YBa_3Cu_4O_{9\pm\varepsilon}$ (*26*); the oxygen stoichiometry around both center copper atoms is not easy to determine and image simulation would not allow one to distinguish between square planar coordination and a statistical occupation of the oxygen in the copper plane when it does not induce deformation of the cation framework (*28*).

The second model was proposed by Ramesh *et al.* who studied the decomposition of $YBa_2Cu_4O_8$ bulk samples (*29*). The authors observe a defect structure which corresponds to the transformation: $YBa_2Cu_4O_8 + YBa_2Cu_4O_8 \rightarrow YBa_2Cu_3O_7 + YBa_2Cu_5O_9$. A wider slab structure is built up from three CuO slabs, i.e., three rows of edge-sharing CuO_4 square planar groups, between CuO_5 pyramids (Fig. 15d).

Distinction between models $YBa_3Cu_4O_9$ and $YBa_2Cu_5O_9$, both chemically satisfactory, is not easy to make. As a first clue, the observed variations of the width of defective slabs in our samples favor the first one, $YBa_3Cu_4O_{9\pm\varepsilon}$, where an oxygen nonstoichiometry is possible around the center coppers (Fig. 15c). Image simulations of both models will only be indicative, cation arrangement being the most important factor (theoretical models give the same parameters with $c = 1.54$ nm). Nevertheless, some calculations have been performed for both structural models. They are based on the same cation positions (in [100] projection) and only differ by the nature of the center cation, Ba in $YBa_3Cu_4O_{9\pm\varepsilon}$ or Cu in $YBa_2Cu_5O_9$. Comparison of observed and calculated through-focus series and especially images where barium sites are highlighted do not invalidate our interpretation hypothesis, $YBa_3Cu_4O_{9\pm\varepsilon}$ is probably the structure of the defective slabs. Crystal images also show numerous Moiré patterns which are probably related to the local superimposition of both lattices, i.e., **124** and **134.** To date, the $YBa_3Cu_4O_9$ ceramic compound has not been successfully synthesized under classical methods; high oxygen pressure may be a good condition for this synthesis. Another original contrast is observed close to the edge of some crystals (Fig. 16). It is located at the level of $(CuO)_2$ slabs. For focus close to Scherzer, zig-zag bright dots associated with oxygen atoms of the intermediate (CuO) layer become bigger and move slightly apart. This contrast is also observed on the edge of crystals showing the 1.5-nm periodicity (Fig. 17). Despite the perturbed image which never extends more than a few nanometers, through-focus series let us associate this contrast to the defect structure at the superimposition and/or junction between $YBa_3Cu_4O_9$ and $YBa_2Cu_4O_8$ areas. This contrast has often been encountered in $YBa_2Cu_4O_8$ samples and tends to prove that this intergrowth defect is not that difficult to stabilize.

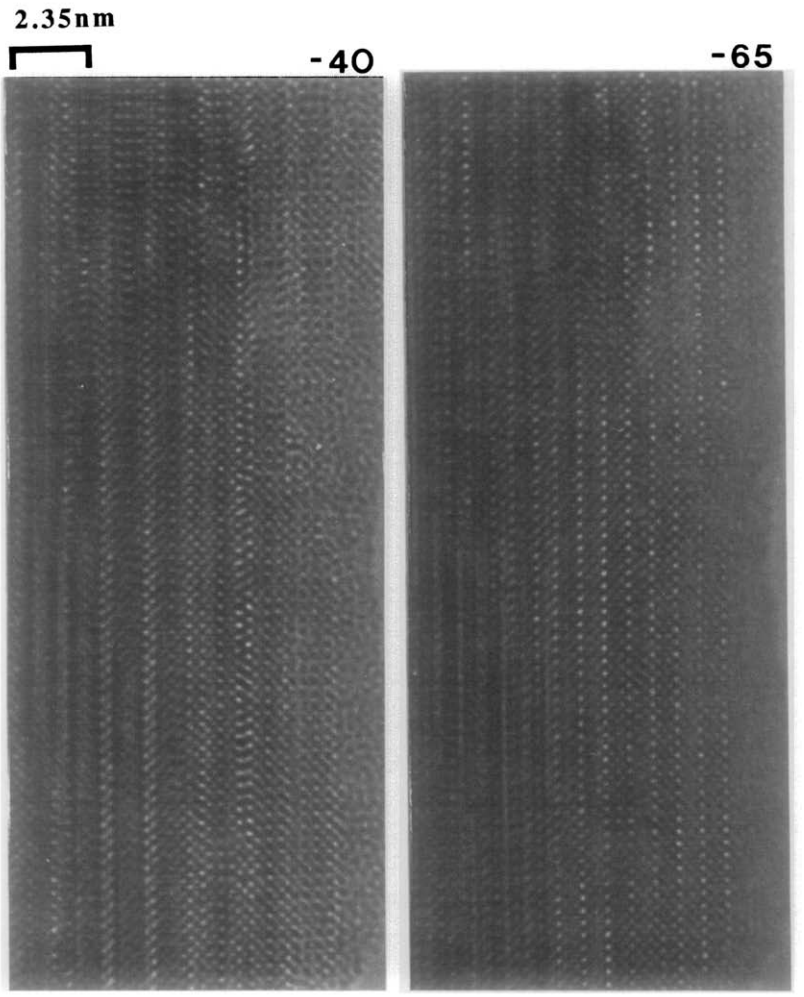

FIG. 17. [100] high resolution images of a defective crystal showing **134** slabs. At the $(CuO)_2$ square planar group level, a similar contrast to that in the previous image is observed at a focus close to −40 nm. As an example in the through-focus series, a −65-nm image suggests at the defect structure the superimposition and/or junction between the $YBa_3Cu_4O_9$ and the $YBa_2Cu_4O_8$ areas.

Conclusion

This study shows that crystals of $YBa_2Cu_4O_8$ prepared under high oxygen pressure are far from being free of defects, the frequency of which seems to be strongly related to the synthesis method. It is worth pointing out that extended disorders are currently observed for which no model can be given. Besides these growth defects, the stacking defects which imply a change in direction of slab stacking exhibit some similarity with the twinning phenomena observed in $YBa_2Cu_3O_7$. Nevertheless they are very rarely obtained compared to twin boundaries in the **123** phase, in agreement with the fact that they involve a strong distortion of the polyhedra at the junction between two 90°-oriented domains except for (001) boundaries, the low frequency of

which directly depends on the synthesis technique. In the same way, the stacking defects which are characterized by only a change in periodicity vary with the pressure of oxygen used during synthesis. The more numerous defects suggest the possible existence of a new phase $YBa_3Cu_4O_9$, whose synthesis should be investigated under high oxygen pressure. It will be important to try to correlate flux pinning in the Y–Ba–Cu–O system with the nature of these defects.

Acknowledgment

The authors are very grateful to Dr. A. Maignan for magnetic measurements.

References

1. B. Domengès, M. Hervieu, C. Michel, and B. Raveau, *Europhys. Lett.* **4,** 211 (1987).
2. H. W. Zandbergen, R. Gronsky, K. Wang, and G. Thomas, *Nature* **331,** 596 (1988).
3. A. F. Marshall, R. W. Barton, K. Char, A. Kapitulnik, B. Oh, R. H. Hazmond, and S. S. Laderman, *Phys. Rev. B* **37,** 9353 (1988).
4. K. Char, M. Lee, W. Barton, A. F. Marshall, I. Bozovic, R. H. Hammond, M. R. Beasley, T. H. Geballe, A. Kapitulnik, and S. S. Laderman, *Phys. Rev. B* **38,** 834 (1988).
5. J. Karpinski, E. Kaldis, E. Jilek, S. Rusiecki, and B. Bucher, *Nature* **336,** 660 (1988).
6. P. Fischer, J. Karpinski, E. Kaldis, E. Jilek, and S. Rusiecki, *Solid State Commun.* **69,** 531 (1989); **70** (1989).
7. R. J. Cava, J. J. Krajewski, W. F. Peck, Jr., B. Batlogg, L. W. Rupp, Jr., R. M. Fleming, A. C. W. P. James, and P. Marsh, *Nature* **338,** 328 (1989).
8. S. Jin, H. M. O'Bryan, P. K. Gallagher, T. H. Tufel, R. J. Cava, R. A. Fastnacht, and G. W. Kammlott, *Physica C* **165,** 415 (1990).
9. S. Jin, T. H. Tiefel, S. Nakahena, J. E. Graebner, H. M. O'Bryan, R. A. Fastnacht, and G. W. Kammlott, *Appl. Phys. Lett.* **56,** 1287 (1990).
10. D. J. Li, J. P. Zhang, L. C. Qin, and L. D. Marks, *in* "Proceedings of the XIIth International Congress for Electron Microscopy," Vol. 4, p. 54 (1990).
11. R. Ramesh, D. M. Hwang, T. Venkatesan, T. S. Ravi, L. Nazar, A. Inam, X. D. Xu, B. Dutta, G. Thomas, A. F. Marshall, and T. H. Geballe, *Science* **247,** 57 (1990).
12. R. Ramesh, D. M. Hwang, T. S. Ravi, C. C. Chang, L. Nazar, T. Venkatesan, A. Inam, X. D. Wu, and B. Dutta, submitted for publication.
13. T. S. Ravi, R. Ramesh, D. M. Hwang, X. D. Wu, A. Inam, and T. Venkatesan, *in* "Proceedings of the XIIth International Congress for Electron Microscopy," Vol. 4, p. 56 (1990).
14. A. F. Marshall, *in* "Proceedings of the XIIth International Congress for Electron Microscopy," Vol. 4, p. 38 (1990).
15. K. Yamaguchi, T. Miyatake, T. Takata, S. Gotoh, N. Koshizuka and S. Tanaka, *Jpn. J. Appl. Phys.* **28,** 1942 (1989).
16. K. Yamaguchi, T. Miyatake, T. Wada, N. Suzuki, T. Takata, N. Koshizuka, H. Yamauchi, and S. Tanaka, *Physica C* **169,** 289 (1990).
17. K. B. Alexander, R. K. Williams, and S. J. Pennycook, *in* "Proceedings of the XIIth International Congress for Electron Microscopy," Vol. 4, 106 (1990).
18. T. Krekels, G. Van Tendeloo, S. Amelinckx, D. M. De Leuuw, and M. De Kraan, *Physica C* **169,** 457 (1990).
19. M. O'Keefe, P. R. Buseck, and S. Iijima, *Nature* **234,** 322 (1978).
20. P. Marsh, R. M. Fleming, M. L. Mandich, A. M. De Santolo, J. Kwo, M. Hongaud, and L. J. Martinez-Miranda, *Nature* **334,** 141 (1988).
21. M. A. Beno, L. Soderholm, D. W. Capone II, D. G. Hinks, J. D. Jorgensen, J. D. Grace, I. K. Schuller, C. U. Segre, and K. Zhang, *Appl. Phys. Lett.* **51,** 57 (1987); J. J. Capponi, C. Chaillout, A. W. Hewat, P. Lejay, M. Marezio, N. Nguyen, B. Raveau, J. L. Soubeyroux, J. L. Tholence, and R. Tournier, *Europhys. Lett.* **12,** 301 (1987).
22. L. Teske and H. K. Müller-Buschbaum, *Z. Anorg. Allg. Chem.* **371,** 325 (1969).
23. N. Kimizuki, E. Takayama, S. Horiuchi, A. Yamamoto, and T. J. Fujita, *J. Solid State Chem.* **42,** 322 (1982).
24. M. Hervieu, B. Domengès, C. Michel, J. Provost, and B. Raveau, *J. Solid State Chem.* **71,** 263 (1987).
25. A. Ourmazd, J. A. Rentschler, J. C. H. Spence, M. O'Keeffe, R. J. Graham, D. W. Johnson, Jr., and W. W. Rhodes, *Nature* **327,** 308 (1987).
26. M. Hervieu, B. Domengès, B. Raveau, M. Post, W. R. McKinnon, and J. M. Tarascon, *Mater. Lett.* **8,** 73 (1989).
27. L. Errhako, C. Michel, P. Lacorre, and B. Raveau, *J. Solid State Chem.* **73,** 531 (1988).
28. B. Domengès, Thèse d'Etat (1989).
29. R. Ramesh, S. Jin, and P. Marsh, *Nature* **346,** 420 (1990).